Counterion Distribution and ζ-Potential in PAMAM Dendrimer

ARTICLE *in* MACROMOLECULES · JULY 2008

Impact Factor: 5.8 · DOI: 10.1021/ma7025435

2 AUTHORS:

Prabal K Maiti
Indian Institute of Science
117 PUBLICATIONS **2,567** CITATIONS
SEE PROFILE

René Messina
University of Lorraine
61 PUBLICATIONS **1,493** CITATIONS
SEE PROFILE

Counterion Distribution and ζ-Potential in PAMAM Dendrimer

Prabal K. Maiti*,† and René Messina‡,§

Center for Condensed Matter Theory, Department of Physics, Indian Institute of Science, Bangalore, India, 560012; Institut für Theoretische Physik II, Heinrich-Heine-Universität Düsseldorf, Universitätsstrasse 1, D-40225 Düsseldorf, Germany

Received November 15, 2007; Revised Manuscript Received April 18, 2008

ABSTRACT: Using several hundred nanosecond long fully atomistic molecular dynamics simulations, we investigate the monomer and counterion local concentrations in poly amido amide (PAMAM) dendrimer systems for various generations at neutral pH. We also calculate the ζ potential as a function of dendrimer generation. It is found that the ζ potential increases with dendrimer generation, but *slowly* at high generation. The ζ potential behavior is remarkably well reproduced when employing Monte Carlo simulations and the Poisson−Boltzmann theory for *colloidal* particles with size and effective charge of the dendrimer as relevant input parameters from the fully atomistic simulations.

I. Introduction

pH responsive charging and swelling phenomena and the high water absorption property of the PAMAM dendrimer make this polymeric material attractive for various technical applications.[1–3] The pH-dependent swelling property can be used for therapeutic applications. Drug molecules can be encapsulated within internal cavities of the dendrimer at low pH which will get released due to a decrease in size at physiological pH.[4] At physiological pH, due to protonation of the primary amines, the PAMAM dendrimer is positively charged. Therefore, they can effectively bind negatively charged DNA and can be used as gene delivery materials.[5–10] The electrostatic binding is largely dependent on the ionic concentration, the pH of the solvent, and the effective surface charge density of the dendrimer. A number of simulation study exists where electrostatic complexation of model dendrimer and polyelectrolyte have been studied.[11,12] Recently, using fully atomistic MD simulation we have demonstrated the electrostatic binding of DNA on PAMAM dendrimer of various generation at various charge ratio.[13] However there is no systematic study of the effective surface charge and the resulting ζ potential as a function of dendrimer generation. The ζ potential is a very important quantity as far as the binding of dendrimer with other oppositely charged polyelectrolytes is concerned since it governs the stability of the complex, its interaction with the cell membrane and the resulting transfection efficiency during delivery. Several experimental studies exist where attempts have been made to obtain ζ potential from the electrophoretic mobility of various types of dendrimer.[14,15] However, from these electrokinetic experiments it is not possible to directly measure the ζ potential. Instead, the ζ potential is obtained from the estimated electrophoretic mobility within a model assumption where the effective surface charge density of the dendrimer is required.

The influence of the generation on the counterion condensation is another area which has not been addressed either experimentally or theoretically. Nevertheless, the counterion distribution for a generic model dendrimer with charged terminal monomers in a salt-free solution was examined by coarse-grained molecular dynamics (MD) simulations for G4 dendrimers.[16] Using a mean field theory, Khokhlov et al. have looked at the influence of the dendrimer effective charge on the counterion density distribution for a generic model of poly(propyleneimine) G5 dendrimer.[17] Very recently, Chen et al. [18] using small angle neutron scattering have investigated the effective charge of G4 PAMAM dendrimer at various pH levels. Employing fully atomistic simulation, earlier we have reported the condensation of counterions on the dendrimer surface and shown how they govern the swelling behavior of PAMAM dendrimer in explicit water.[19] However, we did not perform a systematic study about the effect of dendrimer generation.[19] In this paper, we study the counterion condensation and the ζ potential as a function of dendrimer generation. A comparison for the ζ potential with the Poisson−Boltzmann theory and Monte Carlo (MC) simulations with implicit solvent for *colloidal* particles is provided.

The paper is organized as follows: Section II is devoted to the computational details for the atomistic and colloidal primitive models. In section III, we present and discuss our results from fully atomistic simulations and colloidal models. A short summary is provided in section IV.

II. Computational Details

A. Full Atomistic Molecular Dynamics. We have carried out MD simulations at room temperature for generation $G = 1$ through $G = 7$. The initial configurations for neutral and charged dendrimers up to generation 7 were taken from our earlier studies.[19–21] Using the LEAP module in AMBER, PAMAM dendrimer of various generations at various protonation levels was immersed in a water box using the TIP3P model for water. The box dimensions were chosen in order to ensure a 10 Å solvation shell around the dendrimer structure. In addition, for the high and low pH cases, some water molecules were replaced by Cl^- counterions in order to neutralize the positive charge on the protonated primary and tertiary amine sites on the dendrimer structures. This procedure resulted in solvated structures, containing 126 258 atoms for high pH, 129 679 atoms for neutral pH and 167 350 atoms for low pH for various protonation levels of G7 dendrimer. MD simulation was performed in periodic boundary conditions using the AMBER7 software suite, using the Dreiding force field.[22] The solvated structures were subjected to 1000 steps of steepest descent minimization of potential energy, followed by another 2000 steps of conjugate gradient minimization. During this minimization the dendrimer structure was kept fixed in their starting conformations using a harmonic constraint with a force constant of

* E-mail: maiti@physics.iisc.ernet.in
† Center for Condensed Matter Theory, Department of Physics, Indian Institute of Science.
‡ Institut für Theoretische Physik II, Heinrich-Heine-Universität Düsseldorf.
§ E-mail: messina@thphy.uni-duesseldorf.de.

10.1021/ma7025435 CCC: $40.75
Published on Web 06/10/2008

Table 1. Input Parameters for the Colloidal Primitive Cell Model

generation	box dimension (MD) [Å]	R [Å]	r_0 [Å]	Z_m
3	48 × 48 × 58	31.7	18.55	26
4	65 × 62 × 68	40.3	23.35	47
5	72.8 × 77 × 72	46.0	27.45	87
6	89 × 107 × 109	62.8	33.85	165
7	116 × 108 × 103	67.5	38.95	314

Table 2. Radius of Gyration of Various Generations of the PAMAM Dendrimers at High and Neutral pH, with the Size Determined from SAXS[26] and SANS[27] Experiments also Shown

	R_g [Å] (this work)		R_g [Å] (experiments)	
generation	high pH	neutral pH	SAXS	SANS
1	7.4	9.4	7.9	
2	11.5	13.6	11.8	
3	12.9	17.2	15.9	
4	16.9	21.7	18.6	
5	20.3	26.1	23.07	24.3
6	24.7	32.5	27.5	
7	30.1	37.57	32.11	34.4

500 kcal/mol/Å ^{2}. This allowed the reorganization of the water molecules to eliminate bad contacts with the dendrimer structure. The minimized structure was then subjected to 45 ps of MD, with 2 fs time step. During the dynamics, the system was gradually heated from 0 to 300 K with harmonic constraints on the solute using the SHAKE method. This was followed by 200 ps constant volume - constant temperature (NVT) dynamics with a temperature-coupling constant of 0.5−1.0 ps on the solute. Finally, 10−20 ns NPT unrestrained production dynamics was carried out with a time constant for heat bath coupling of 1 ps. The volume of the simulation box (average box dimenstions for various generations are given in Table 1) was adjusted to have the correct density corresponding to the NPT ensemble. The electrostatics interactions were evaluated with the particle mesh Ewald[23] (PME) method, using a real space cut off of 9 Å.

B. Colloidal Models. *1. Monte Carlo Simulations of the Primitive Model.* We present now a coarse grained model that is hopefully able to mimic some of the counterion distribution properties found in the fully atomistic simulations described above. The electrostatic model system considered here is similar to that studied in previous works.[24,25] It is made up of two types of charged hard spheres: (i) a macroion of radius r_m (standing for a coarse dendrimer) with a positive bare charge $Q_m = Z_m e$ (with $Z_m > 0$) and (ii) small monovalent counterions of radius $r_c = 2.2$ Å (standing for the negatively charged chlorine ions and obtained from the radial distribution function of terminal nitrogen and chlorine ions) to ensure the electroneutrality of the system. The aqueous solvent (water) enters only via its relative permittivity $\varepsilon_w \approx 80$. Note that all the molecular discrete aspects of the water are omitted. All those related approximations correspond to the so-called primitive model. Measurements were typically performed over 10^6 MC steps per particle.

In order to establish a mapping between the MD simulations and the coarse grained MC simulations, we have adopted the following strategy: The radius R of the spherical simulation box was chosen such that $V = 4/3\pi R^3$, where V denotes the mean volume of the simulation box in MD simulations. The relevant center-center distance of closest approach between the macroion and the counterion, r_0, is given by $r_0 = R_g + r_{NCl}$, where the radius of gyration R_g of the dendrimer is stemming from the MD data (see Table 2 for neutral pH. The little correction $r_{NCl} = 1.35$ Å is due to the bound counterions onto the terminal primary nitrogen and corresponds to the peak in the pair correlation function between Cl^- and terminal nitrogens. Accordingly we have $r_m = r_0 - r_c = R_g + r_{NCl} - r_c$. The number of counterions N is prescribed by the (average) charge enclosed within a radius R_g from the center of mass of the dendrimer found in the MD calculations (i.e., $N = Z_m$). Our simulation run parameters are given in Table 1.

2. Poisson−Boltzmann theory. To further enrich our study, we have also considered the mean-field Poisson−Boltzmann (PB) theory. In the PB theory the divergence of the electric field (or equivalently the Laplacian of the mean electrostatic potential ϕ) is directly proportional to the charge density, where the latter is assumed to obey a Boltzmann distribution. More precisely, we have numerically solved the following nonlinear integro-differential equation for the (radial) electric filed $E(r)$:

$$\frac{1}{r^2}\frac{\partial(r^2E)}{\partial r} = -\frac{en_0}{\varepsilon_0\varepsilon_w}\exp\left[\beta e\int_{r_0}^{r} E(r')\,dr'\right] \quad (1)$$

where n_0 (which has the dimension of a volume density) must verify the electroneutrality condition

$$n_0\int_{r_0}^{R} 4\pi r^2 \exp\left[\beta e\int_{r_0}^{r} E(r')\,dr'\right] dr = Z_m \quad (2)$$

which implicitly imposes $E(R) = 0$. The second needed boundary condition is also a consequence from the Gauss law and yields $E(r_0) = Z_m e/\epsilon_0\varepsilon_w 4\pi > r_0^2$.

In practice, we start with a (discrete) linear profile for $E(r)$ where the boundary conditions are met at the two fixed end points $r = r_0$ and $r = R$. The profile of $E(r)$ is iteratively updated (except the two fixed end points) via eqs 1 and 2 until convergence is reached. Using a "mixed" solution consisting of a linear combination of the new profile and the old one, the convergence is very fast. The relevant input parameters are merely R, r_0, and Z_m. Once the profile of $E(r)$ is obtained, the one of $\phi(r)$ is also known, via a straightforward integration. At this stage, all the relevant observables, especially the ζ potential, can be determined.

III. Results and Discussion

A. Conformational Properties. The mean squared radius of gyration R_g^2 provides an adequate measure of the conformational change of the dendrimer upon varying the protonation level at prescribed dendrimer generation. In Figure S1 of the Supporting Information we show the time evolution of the R_g for G3 and G7 at neutral pH to show the conformational relaxation. Table 2 gives an overview of the measured radii of gyration R_g at high and neutral pH conditions for PAMAM dendrimer up to generation 7. For comparison, we also provide the radii of gyration obtained from Small angle X-ray scattering (SAXS)[26] and Neutron scattering (SANS)[27] experiments. The SAXS experiments were performed in dilute solution of PAMAM dendrimers in methanol solution which corresponds to high pH. It is clearly observed from our simulation data (see Table 2) that the dendrimer swells upon decreasing the pH, as a direct consequence of the higher degree of protonation at neutral pH. For the high pH case, our simulation data from this present work are in good quantitative agreement with the experimental ones as well as with the earlier published simulation results.[19] This pH dependent swelling has been earlier studied by MC simulation[28] and atomistic MD simulation.[2,19]

B. Counterion and Monomer Distribution. We consider here *neutral* pH conditions at which all the primary amines of the PAMAM dendrimer are protonated. In Figure 1, we show the equilibrium snapshot of the G3 and G7 dendrimer at neutral pH. The surrounding Cl^- ions are shown in green. To emphasize the location of the counterions with respect to the dendrimer we have also shown the charged amine sites in blue spheres, see Figure 1. A significant number of counterions are localized deep inside the dendrimer and very close to (within 10−15 Å for G7) the center of mass of the dendrimer; see Figure 1.

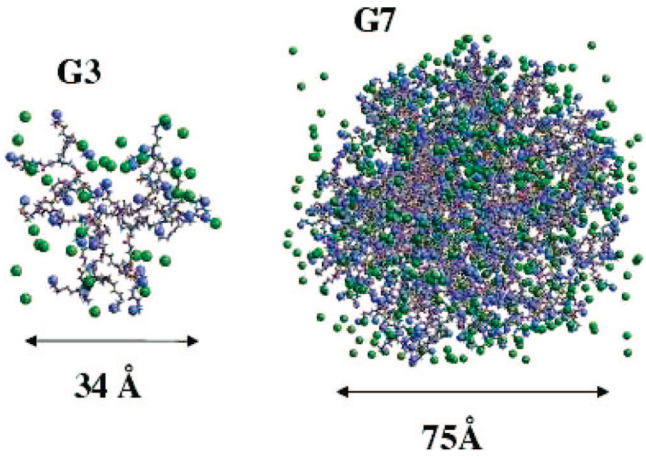

Figure 1. Snapshots of typical equilibrium configurations of G3 and G7 dendrimers at neutral pH. The protonated amine sites are are shown in blue, and the Cl^- ions are shown in green.

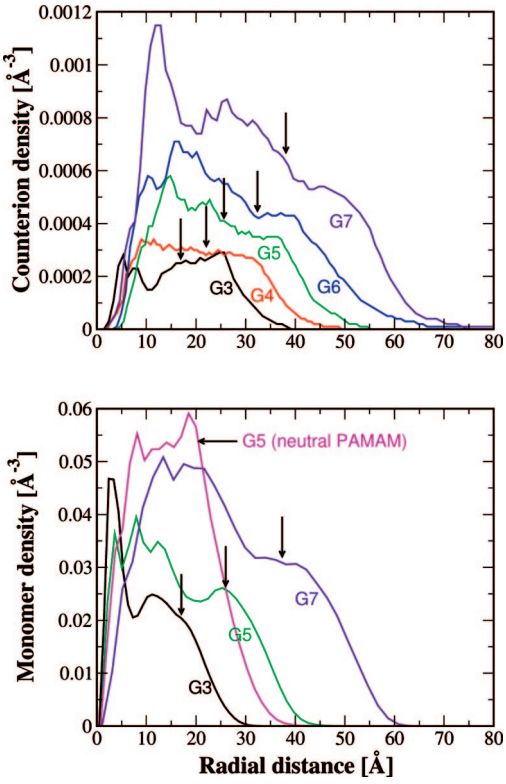

Figure 2. Counterion and monomer density profiles for various generations of the PAMAM dendrimer at neutral pH when all the primary amines are protonated. The arrows indicate the radial distance corresponding to R_g. For comparison, we have also added the monomer density distribution of neutral G5 dendrimer at high pH.

The average *radial* ion (counterion or monomer) density $\bar{n}(r)$, with r denoting the distance between the center of mass of an ion and the center of mass of the dendrimer, can be defined by counting the number of ions whose centers of mass are located within the spherical shell of radius r and thickness dr. The (*local*) counterion density $\rho(r)$ is merely related to the radial one via $\rho(r) = \bar{n}(r)/4\pi > r^2$.

Figure 2 shows the (local) counterion and monomer density profiles for various generations of the PAMAM dendrimer in water at neutral pH conditions. A remarkable feature is that, in the direct vicinity of the center of mass (within 5 Å), the monomer density decreases with growing generation; see Figure 2. This nontrivial effect was also recently reported by Opitz and Wagner[29] in their fully atomistic simulations using explicit solvent. A similar behavior was also observed by Götze and Likos,[30] who investigated neutral flexible dendrimers by means of coarse-grained Monte Carlo simulations. They attributed this effect to the sharper localization of the center-of-mass of the dendrimer in the middle of the core where no monomers reside for higher generation dendrimer. For smaller generation, due to less crowding of the interior and larger conformational fluctuations, the center-of-mass can occasionally coincide with the monomer at the core and hence give rise to a larger monomer density near the core. We can envisage a similar scenario here which gives rise to the observed monomer distribution. Another important feature of the monomer density distribution is the appearance of a minimum at around 10−15 Å away from the core for G3−G4 and the location at which this minimum occurs shifts to higher distance with increasing generation (at around 20 Å away from the core for G5 and G6). To better elucidate the possible role of the counterions, we have checked that in the case of high pH (corresponding to a neutral dendrimer without counterions), the local monomer density does not exhibit this minimum (see Figure S2 in the Supporting Information). This indicates that the presence of counterions dramatically influences the monomer distribution and promotes layering.

As far as the counterion distribution is concerned, Figure 2 reveals a significant counterion penetration in the interior of the dendrimer. At radial distances larger than about 10 Å, corresponding roughly to the value of R_g for the first internal generation, it can be seen that the counterion density significantly increases with growing generation, see Figure 2. These observations can be rationalized with simple ideas: Upon increasing the generation the amount of monomers stemming from *backfolding* is getting higher (as deduced from the monomer density profiles plotted in Figure 2), and therefore, more counterions are required to screen the excess polymeric charge near the core. Notice that backfolding is only entropically favorable, but electrostatically unfavorable when there are no counterions present as in the case of high pH. However, when the electrostatic penalty is reduced upon counterion condensation (or accumulation), a subtle interplay between chain-entropy and electrostatics sets in which governs the chain conformations.

C. ζ Potential. An interesting and experimentally widely measured quantity is the so-called ζ potential. Typically, it is the electrophoretic mobility that is directly accessible experimentally. The ζ potential is then obtained via a model in an indirect manner. Recently, Diehl and Levin[31] argued, using the Smoluchowski equation and MC simulations, that the shear plane, at which the ζ potential should be identified within the mean electrostatic potential [$\phi(r)$], must be placed at least one ionic diameter away from the colloidal surface. Doing so,[31] an important feature, such as the charge reversal, is signaled by a switch of the sign of the ζ potential as it is experimentally the case. We have followed those lines[31,32] and extracted the value of the ζ potential from the profile of $\phi(r)$ as $\zeta = \phi(R_g + 2r_c) = \phi(r_0 + r_c)$. For the MD data, we compute the profile of $\phi(r)$ via a double integration of the charge density profile (stemming merely from the Poisson equation). The ζ potential is then obtained by considering $\zeta = \phi(R) - \phi(r_0 + r_c)$, where R is the radius of the inscribed sphere within the rectangular MD simulation box. Hence for all the calculations (MD, MC and PB) we have the same "fictitious" shear radius of $r_0 + r_c$, making the comparison between the different approaches consistent.

Our results for the ζ potential are depicted in Figure 3. The agreement between the different approaches is remarkable. The ζ potential *increases* with growing generation. This feature is consistent with the intuitive idea that the bare charge Q_{bare} (i.e., omitting the counterions inside the dendrimer) at neutral pH increases exponentially with the generation. To be more specific, the bare charge grows as $Q_{bare}/e = c2^G$, where $c = 4$ is the

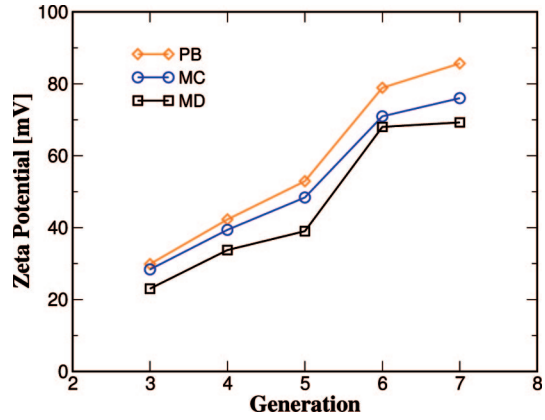

Figure 3. ζ potential as a function of the dendrimer generation for the Poisson−Boltzmann (PB), Monte Carlo (MC), and molecular dynamics (MD) calculations.

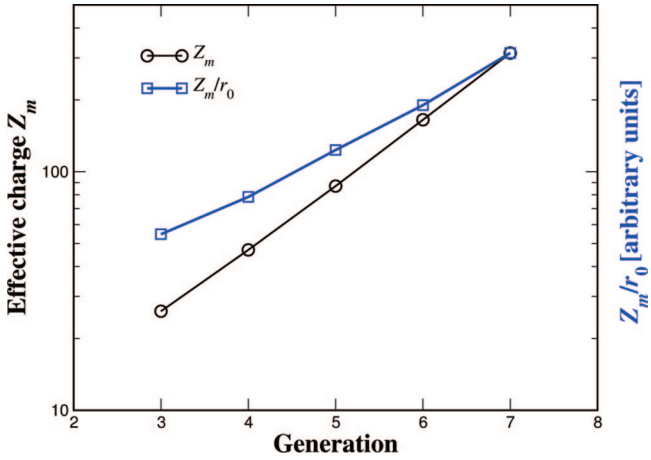

Figure 4. Effective charge Z_m and bare contact potential Z_m/r_0 as a function of the dendrimer generation.

number of branches of the core. To better understand the role of the condensed counterions *inside* the dendrimer we have plotted the (reduced) effective charge Z_m as well as Z_m/r_0 as a function of the generation number (see Table 1 for the values of Z_m and r_0) in Figure 4. An exponential behavior is also indeed exhibited for the effective charge Z_m (see Figure 4). Consequently, the condensed counterions inside the dendrimer do not affect the exponential behavior of the effective charge with respect to the generation. If one further assumes that the radius of gyration scales roughly exponentially with the generation, then the bare potential at contact $\phi_0 \sim Q_{\text{bare}}/r_0$ should present an exponential-like growth as well. This latter feature is also (qualitatively) found in Figure 4 for Z_m/r_0.

Therefore the nonexponential behavior of the ζ potential reported in Figure 3 is exclusively due to the counterions living *outside* the dendrimer. MD data also suggests a saturation of the ζ potential at high generation number (see Figure 3). This trend is qualitatively reproduced by the primitive model (PB and MC data), where we find a considerable attenuation of the increase of the ζ potential (see Figure 3). Also, the jump in the ζ potential in going from generation 5 to 6 is observed for all the three cases namely PB, MC, and MD data (see Figure 3). These findings lead to the important conclusion that the a knowledge of the effective charge and the size of the PAMAM dendrimer at neutral pH is enough to capture the realistic behavior of the ζ potential within an electrostatic model as simple as the PB theory.

IV. Concluding Remarks

To summarize, we have performed several hundred nanosecond long fully atomistic molecular dynamics simulations to study the pH responsive behavior of PAMAM dendrimer at varying pH. We have emphasized the counterion distribution and the ζ potential at neutral pH corresponding to a salt-free system. It was demonstrated that the counterions can significantly penetrate the dendrimer. The local counterion concentration within the dendrimer increases with growing dendrimer generation. This feature is due to higher degree of backfolding at higher generations and charge screening by counterions. As far as the ζ potential of the dendrimer is concerned, we have shown that it increases slowly with growing generation, in contrast to the exponential behavior of the bare surface potential. A remarkable agreement is obtained, when compared to colloidal models with an effective charge and size as input parameters from the fully atomistic MD simulations. This constitutes the first theoretical calculation of the ζ potential for the PAMAM dendrimer, and more generally to dendrimeric systems. It is worth to mention that an estimate of the effective charge of the PAMAM dendrimer was recently provided in SANS experiments,[18] giving support to our theoretical approach.

Acknowledgment. We are grateful to Yan Levin for very fruitful discussions. P.K.M. acknowledges financial support from the Alexander von Humboldt foundation and thanks R. Netz for warm hospitality. R.M. thanks the Center for Condensed Matter theory, Indian Institute of Science, for hospitality and acknowledges financial support from the DFG via Grants LO418/12 and SFB TR6.

Supporting Information Available: Figures showing the radius of gyration as a function of time for G3 and G7 PAMAM dendrimers and monomer density profiles for G3-G7 PAMAM dendrimers at high pH. This material is available free of charge via the Internet at http://pubs.acs.org.

References and Notes

(1) Bielinska, A. U.; KukowskaLatallo, J. F.; Baker, J. R. *Biochim. Biophys. Acta* **1997**, *1353*, 180.
(2) Lee, I.; Athey, B. D.; Wetzel, A. W.; Meixner, W., Jr *Macromolecules* **2002**, *35*, 4510.
(3) Ottaviani, M. F.; Furini, F.; Casinii, A.; Turro, N. J.; Jockusch, S.; Tomalia, D. A.; Messori, L. *Macromolecules* **2000**, *33*, 7842.
(4) Bosman, A. W.; Janssen, H. M.; Meijer, E. W. *Chem. Rev.* **1999**, *99*, 1665.
(5) KukowskaLatallo, J. F.; Bielinska, A. U.; Johnson, J.; Spindler, R.; Tomalia, D. A.; Baker, J. R. *Proc. Natl. Acad. Sci. U.S.A.* **1996**, *93*, 4897.
(6) Kabanov, V. A.; Zezin, A. B.; Rogacheva, V. B.; Gulyaeva, Z. G.; Zansochova, M. F.; Joosten, J. G. H.; Brackman, J. *Macromolecules* **1998**, *31*, 5142.
(7) Haensler, J.; Szoka, F. C. *Bioconjugate Chem.* **1993**, *4*, 372.
(8) Zinselmeyer, B. H.; Mackay, S. P.; Schätzlein, A. G.; Uchegbu, I. F. *Pharm. Res.* **2002**, *19*, 960.
(9) Dufés, C; Uchegbu, I. F.; Schätzlein, A. G. *Adv. Drug Delivery Rev.* **2005**, *57*, 2177.
(10) Santhakumaran, L. M.; Thomas, T.; Thomas, T. J. *Nucl. Acid. Res.* **2004**, *32*, 2102.
(11) Welch, P.; Muthukumar, M. *Macromolecules* **2000**, *33*, 6159.
(12) Lyulin, S. V.; Darinskii, A. A.; Lyulin, A. V. *Macromolecules* **2005**, *38*, 3990.
(13) Maiti, P. K.; Bagchi, B. *Nano Lett.* **2006**, *6*, 2478.
(14) Huang, Q. R.; Dubin, P. L.; Moorefield, C. N.; Newkome, G. R. *J. Phys. Chem. B* **2000**, *104*, 898.
(15) Welch, C. F.; Hoagland, D. A. *Langmuir* **2003**, *19*, 1082.
(16) Gurtovenko, A. A.; Lyulin, S. V.; Karttunen, M.; Vattulainen, I. *J. Chem. Phys.* **2006**, *124*, 094904.
(17) Govorun, E. N.; Zeldovich, K. B.; Khokhlov, A. R. *Macromol. Theory Simul.* **2003**, *12*, 705.
(18) Chen, W.; Porcar, L.; Liu, Y.; Butler, P. D.; Magid, L. J. *Macromolecules* **2007**, *40*, 5887.
(19) Maiti, P. K.; Lin, S. T.; Cagin, T.; Goddard, W. A., III *Macromolecules* **2005**, *38*, 979.

(20) Maiti, P. K.; Cagin, T.; Wang, G. F.; Goddard, W. A., III *Macromolecules* **2004**, *37*, 6236.
(21) Lin, S. T.; Maiti, P. K.; Cagin, T.; Goddard, W. A., III *J. Phys. Chem. B* **2005**, *109*, 8663.
(22) Mayo, S. L.; Olafson, B. D.; Goddard, W. A., III *J. Phys. Chem. B* **1990**, *94*, 8897.
(23) Darden, T.; York, D.; Pedersen, L. *J. Chem. Phys.* **1993**, *98*, 10089.
(24) Messina, R. *J. Chem. Phys.* **2002**, *117*, 11062.
(25) Barbosa, M. C.; Deserno, M.; Holm, C.; Messina, R. *Phys. Rev. E* **2004**, *69*, 051401.
(26) Rathgeber, S.; Monkenbusch, M.; Kreitschmann, M.; Urban, V.; Brulet, A. *J. Chem. Phys.* **2002**, *117*, 4047.
(27) Topp, A.; Bauer, B. J.; Tomalia, D. A.; Amis, E. J. *Macromolecules* **1999**, *32*, 7232.
(28) Welch, P.; Muthukumar, M. *Macromolecules* **1998**, *31*, 5892.
(29) Opitz, A. W.; Wagner, N. J. *J. Polym. Sci., Part B: Polym. Phys.* **2006**, *44*, 3062.
(30) Götze, I. O.; Likos, C. N. *Macromolecules* **2003**, *36*, 8189.
(31) Diehl, A.; Levin, Y. *J. Chem. Phys.* **2006**, *125*, 054902.
(32) We admit that there is some arbitrariness upon choosing the location of the shear plane. Nonetheless, the results should not qualitatively change within one ionic radius interval.

MA7025435